

Lasing behavior modulation in a layered cylindrical microcavity

Panlin Li · Chunxiang Xu · Mingming Jiang · Jun Dai ·
Jitao Li · Junfeng Lu

Received: 6 July 2014 / Accepted: 30 October 2014 / Published online: 12 November 2014
© Springer-Verlag Berlin Heidelberg 2014

Abstract Optically pumped lasing behaviors modulation was realized in a layered cylindrical microcavity dye laser formed by rhodamine 6G-doped quinoline in a capillary. By inserting an optical fiber into the cylindrical microcavity, whispering gallery modes were successfully suppressed and a new kind of waveguide mode lasing was obtained. The lasing characteristics and resonance mechanism of the two configurations were systematically discussed in both experiment and theoretical calculation. Moreover, the time domain and frequency domain finite element methods were performed and found that with the adjustment of the central fiber, the transition of resonant mode from WGMs to waveguide modes can be achieved.

1 Introduction

Optical microresonators have proven to be highly important for both fundamental physics investigation of light–matter interaction [1] and potential applications such as efficient microlaser, optical filters, modulators, and miniature sensors [2–5]. To date, various types of microresonators, such as Fabry–Pérot cavity [6, 7], random cavity [8], plasmonic cavity [9], distributed feedback (DFB) resonator [10], as well as whispering gallery mode (WGM) cavity [11, 12],

have been proposed and demonstrated. Among these alternatives, the WGM microcavities have attracted increasing research attention in recent years due to their low optical losses and tight mode confinement. In such resonators, light wave is guided by continuous total internal reflection (TIR) at the cavity boundary. When the round trip optical path length is equal to an integer number of the light wavelength, constructive interference of light takes place inside the WGM microcavity.

WGM lasing from various geometries, including microspheres [13, 14], microrings [15, 16], and microcylinders [17, 18], have been reported. For spherical resonators such as microdroplets, laser emission can be generated by embedding gain materials into such cavity [13], while for the microring cavities, the WGM lasing is obtained by coating a polymer gain layer around the optical fiber [16]. However, the difficulty in manipulation and mechanical fragility largely hinder their practical applications. Obviously, the layered cylindrical microcavity consisting of a fused-silica capillary filled with a high refractive index (RI) liquid might be favorable for WGM lasing in terms of both simpler fabrication and better mechanical stability. Moreover, capillary cavities are easier to be aligned into arrays and readily compatible with microfluidic systems [19].

Besides the high quality performance, laser modulation capability is also required in the application of modern technologies such as tunable optical sources and optical communication. Generally, laser modulation has been realized by adjusting optical cavity size and shape [20, 21], but mechanical control is inaccurate and impractical for real applications. Another possible scheme indicated by the previous studies [22–24] is using coupled asymmetric microcavity via the Vernier effect. Compared with traditional approaches, the capillary cavities can easily integrate

P. Li · C. Xu (✉) · J. Dai · J. Li · J. Lu
State Key Laboratory of Bioelectronics, School of Biological
Science and Medical Engineering, Southeast University,
Nanjing 210096, China
e-mail: xcxseu@seu.edu.cn

M. Jiang
State Key Laboratory of Luminescence and Applications,
Changchun Institute of Optics, Fine Mechanics and Physics,
Chinese Academy of Sciences, Changchun 130033, China

with other photonic components, which provide an effective route to manipulating the lasing [24, 25]. Herein, we investigated the optically pumped lasing characteristic based on capillary tubes. By inserting an optical fiber into the capillary, lasing spectrum corresponding to the waveguide modes can be achieved. Our approach is proposed to control the laser behaviors based on modulating the optical oscillation path. Correspondingly, the optical field distributions for TE modes were also simulated to illustrate the resonant process by a time domain and frequency domain finite element methods.

2 Experimental section

We used the rhodamine 6G dye (R6G) dissolved in quinoline solution (RI $n_2 = 1.626$ at 20 °C) as the gain medium. The dye concentration was fixed at 1.8×10^{-3} mM/L. The solvent was chosen based on its higher RI than fused-silica capillary ($n_1 = 1.458$ at $\lambda = 600$ nm). Capillaries with different inner radius were dipped into the dye solution to make the mixture infill the tube through the capillary action with no need for external syringe pump. A femtosecond pulse laser operating at 520 nm was focused perpendicular to the capillary axis. The pump power was adjusted with neutral density filter and monitored with an energy meter. The emission from the microcavity was collected by the use of a fiber and coupled into a charge-coupled-device (CCD) array detector in an optical-multichannel analyzer (OMA) system. All of the measurements were performed under ambient conditions.

3 Results and discussion

3.1 WGM lasing without the central fiber

We started by demonstrating a conventional lasing without the central fiber. The experimental setup is shown schematically in Fig. 1. In this case, dye solution has a RI higher than that of the capillary, thus essentially becoming a cylindrical resonator by itself. Figure 2a shows the power-dependent photoluminescence (PL) spectra of a typical capillary microcavity with inner radius of 100 μm . Under low excitation of 6 kW/cm^2 , the emission spectrum displays a weak spontaneous emission with a peak at 580 nm. When a certain threshold is reached, multimode laser emission appears in the longer wavelength range (590–605 nm) of the spontaneous emission spectrum owing to the re-absorption effect [26]. The lasing profile shows continuous blue shift from 605 to 585 nm when the excitation density increases from 14 to 62 kW/cm^2 . Various reasons may

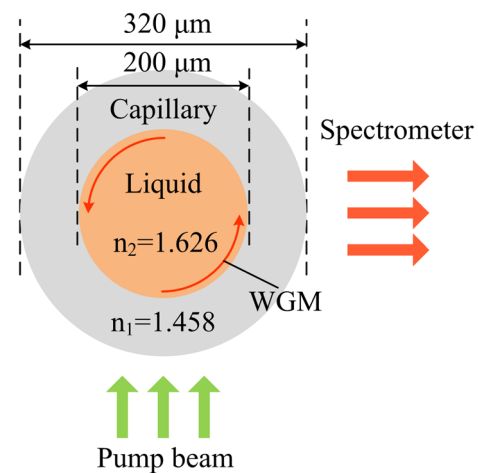


Fig. 1 Schematic cross-sectional view of the experimental setup for optical characterization (The red ring inside capillary indicates WGM)

account for the shift in emission wavelength under higher excitation density: (1) The RI of the quinoline solution. (2) The concentration of the dye solution. (3) The effective cavity size. The effects of each are discussed below.

Since the expansion coefficient of fused silica is negligibly small compared with that of the liquid, the cavity size is independent of the liquid temperature. In addition, since quinoline is a weak volatilized organic liquid, its concentration change can also be ignored. As is well known, any variations in the RI of the gain medium will lead to changes of optical path inside the cavity, therefore resulting in a shift in resonant mode [27]. As the excitation density increases, the effective optical path will decrease due to the decrease of the RI. Hence, we conclude that the changes in emission wavelengths are due to changes in the RI of quinoline.

A plot of integrated emission intensity of the peaks with excitation density is presented in Fig. 2b. The superlinear increase of the emission intensity indicates the lasing behavior with the threshold around 9 kW/cm^2 . Figure 2c–e shows the optical images of the measured capillary. The strong green light at the center is from the pump beam. It is noted that above threshold (Fig. 2e), the emission from the capillary is much brighter compared with the one below threshold (Fig. 2c). Moreover, above threshold, bright red emission from the liquid–capillary interface can be observed in all directions. This predicts that the lasing may come from the WGM laser light escaping tangentially from the inner boundary.

It is noted that each peak (Fig. 2a) contains several sub-peaks. To show the fine spectral structure of the WGM lasing emission, the spectra were recorded with a grating density of 1,800 g/mm and shown in Fig. 3. The full width

Fig. 2 **a** The PL emission of a typical capillary microcavity recorded at room temperature as a function of excitation density. **b** The integrated intensity of emission peak dependence on the excitation density. **c–e** Optical images of the measured capillary below threshold (**c**), near threshold (**d**), and above threshold (**e**)

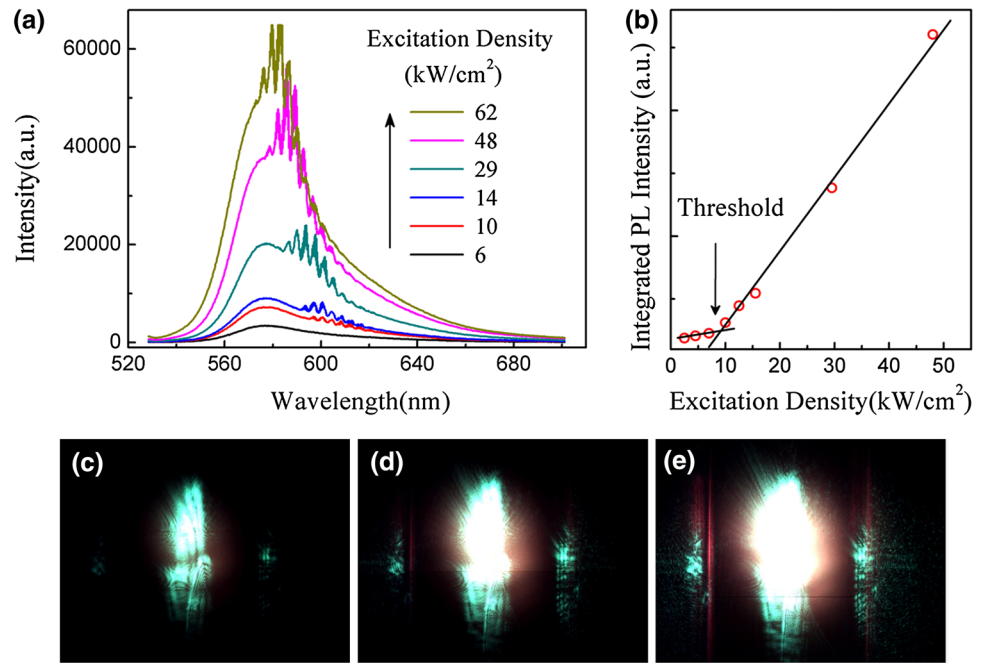
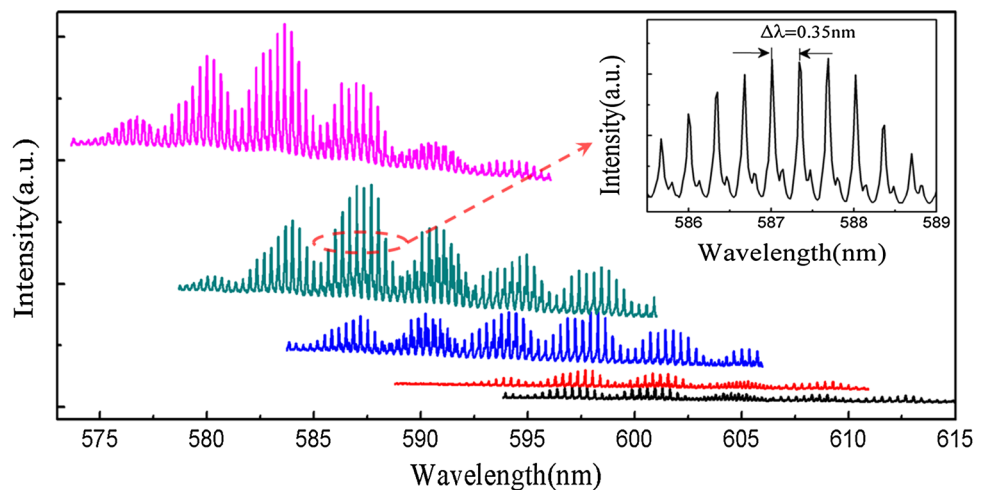


Fig. 3 Lasing spectra recorded with a grating of density: 1,800 g/mm. The excitation densities from low to high are: 10, 14, 29, 48, and 62 kW/cm². The inset shows a portion of the same spectrum under higher resolution



at half-maximum (FWHM) of the mode at ~587.04 nm is 0.05 nm, and the corresponding cavity Q factor is of the order of ~11,700. The mode spacing of the lasing denoted as $\Delta\lambda$ is measured to be 0.35 nm. In general, Q factor of a microcavity monotonically decreases with increasing radial mode order l . Here, we only consider modes with the radial mode order $l = 1$, since those have the highest Q factors for a given angular mode number m [28]. The resonant wavelengths for the WGMs are determined by the following equation

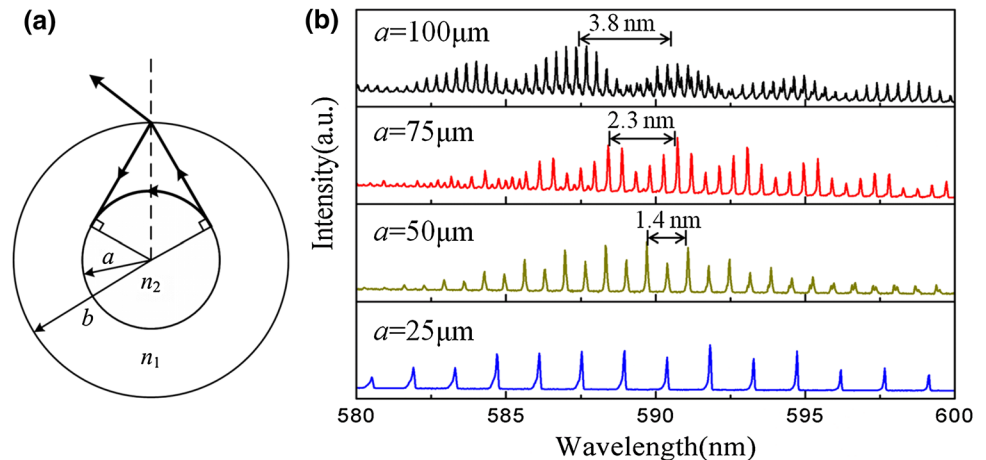
$$m\lambda = 2n\pi a \tag{1}$$

where m , n , and a are integers giving the number of wavelengths in a round trip of the cavity, the effective RI of the liquid, and the inner radius of the capillary, respectively. The wavelength spacing between two adjacent modes (λ_m and λ_{m+1}) can be estimated as [20]

$$\Delta\lambda = \lambda_m - \lambda_{m+1} = \frac{\lambda^2}{2\pi na} \tag{2}$$

For this case, the calculated mode spacing $\Delta\lambda$ is 0.34 nm for $\lambda = 590$ nm and is consistent with the experimental data, which implies that these lasing peaks are attributed to the whispering gallery resonances at the liquid–capillary interface.

Fig. 4 **a** A ray-optic description of interference in a capillary microcavity. The lasing light reflected from the external surface could interfere with the inner WGM. **b** Typical modulated lasing emission spectra from capillaries with different a



3.2 Interference modulation of WGMs

Figure 3 clearly shows another salient characteristic of laser where the lasing modes are periodically modulated in intensity. The wavelength distance $\delta\lambda$ between two locally strong peaks is measured to be 3.8 nm. The intensity modulation phenomenon can be understood by the interference between the WGMs and the reflected light from the capillary wall [29]. The corresponding ray-optic representation is proposed in Fig. 4a. The inner WGM laser light will escape tangentially from the inner boundary, and some light may be reflected from the external surface of the capillary, coupling back into the inner cavity. The reflected light may interfere constructively or destructively with the WGM propagating close to the inner boundary, depending on the difference in optical path length $\Delta L = 2[n_1\sqrt{b^2 - a^2} - n_2a \arccos(a/b)]$ between the two rays per one reflection cycle. Hence, the condition for constructive interference can be approximated as [29]

$$p\lambda = 2[n_1\sqrt{b^2 - a^2} - n_2a \arccos(a/b)] \quad (3)$$

where p is an integer. The period of the interference modulation $\delta\lambda$ is strongly dependent on the geometry size of the capillary.

The intensity modulation characteristics were further investigated by studying lasing spectra of the capillaries with different sizes. Figure 4b plots a series of lasing spectra detected from capillaries with different inner radius. As inner radius a decreases from 100 to 75, 50 μm , the interference period decreases from 3.8 nm to about 2.3, 1.4 nm, respectively. Nevertheless, such optical modulation was not observed when $a = 25 \mu\text{m}$. In the former three cases, the calculated periods for the interference modulation agree well with the experimental data. For instance, at $a = 75 \mu\text{m}$, the optical path length difference ΔL of the two

Table 1 Interference period $\delta\lambda$ comparison between experimental observation and calculation of different capillaries

Radius of capillaries (μm)		Mode spacing $\Delta\lambda$ (nm)		Interference period $\delta\lambda$ (nm)	
a	b	Calculation	Experimental	Calculation	Experimental
99	164	0.34	0.35	4.05	3.8
75	158	0.45	0.46	2.35	2.3
50	160	0.68	0.68	1.45	1.4
24	160	1.42	1.43	1.01	–

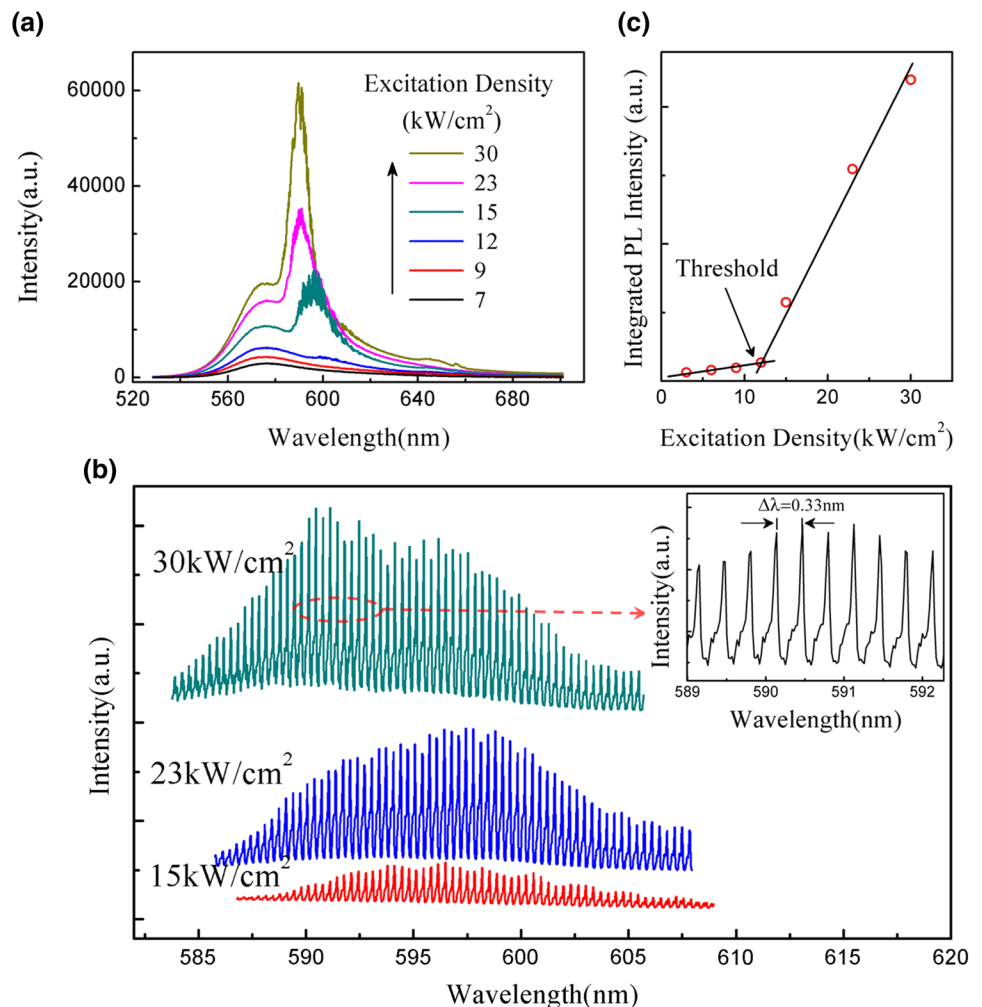
The calculation is based on the Eq. (3)

rays is about 148 μm ; hence, the calculated interference period ($\delta\lambda = \lambda^2 / \Delta\lambda$, $\lambda = 590 \text{ nm}$) of 2.35 nm is consistent with the measured value of 2.3 nm within experimental error. For better comparison between experimental data and theoretical calculation, the interference period ($\delta\lambda$) and mode spacing ($\Delta\lambda$) of the lasing spectra for different capillaries are listed in Table 1. The radii were determined by optical microscopy. As shown in Table 1, the value of mode spacing ($\Delta\lambda$) gradually increases with decreasing inner radius a . This is reasonable based on Eq. (2). Considering that $a = 25 \mu\text{m}$, the prediction of interference period is smaller than the mode spacing ($\delta\lambda = 1.01 < \Delta\lambda = 1.363$). Furthermore, less light is reflected from the external surface of the capillary due to the smaller incident angle. As a result, no noticeable modulation was observed as shown in Fig. 4b.

3.3 Waveguide mode lasing with the central fiber

As discussed earlier, the capillary cavity shows simple liquid handling and optical setting at the micron-sized level. Therefore, it offers us sufficient freedom to modify

Fig. 5 Typical emission spectra recorded by gratings with two different densities: 300 g/mm (a) and 1,800 g/mm (b) of the capillary with the central fiber inserted. c The integrated intensity of emission peak dependence on the excitation density showing a threshold of 12 kW/cm²



the structure [18, 25]. When an optical fiber of 125 μm diameter was inserted in the same capillary (inner radius $a \sim 100 \mu\text{m}$), the emission spectra changed dramatically. For the typical lasing spectra shown in Fig. 5, we made two observations: (1) The degree of the interference modulation is much weaker relative to the modulated spectra in Fig. 3. (2) The mode spacing $\Delta\lambda = 0.33$ nm obtained from the emission peaks in Fig. 5 is smaller than that ($\Delta\lambda = 0.35$ nm) of the whispering gallery resonance occurred at the inner liquid–capillary interface. The path length L for a round trip was calculated as $L = 648 \mu\text{m}$ by using $L = \lambda^2/n_2\Delta\lambda$, which is longer than the circumference of the inner cavity ($L = 2\pi a = 628 \mu\text{m}$).

As the central fiber was inserted, the capillary micro-cavity may support two different types of optical modes: well-known WGMs and waveguide modes. WGMs come from the TIRs of the optical mode along the liquid–capillary interface and escape tangentially from the boundary. As opposed to waveguide modes, the lasing is achieved by successive reflections between the liquid–capillary interface and the outer surface of the fiber. These two types of

resonant cavity mode are depicted schematically using a ray-optic representation seen in Fig. 6.

We tentatively analyze the resonant mechanism based on the waveguide model, as shown in Fig. 6b. Under this assumption, the half angle ϕ of the reflected ray can be calculated as $\phi = \theta - \arcsin(\frac{d}{a} \sin \theta)$, where θ is the incident angle at the boundary of liquid and fiber. The critical angle of total reflection at the boundary of liquid and fiber is calculated to be 64° with $n_{\text{fiber}} = 1.455$, and θ should be larger than the critical angle so as to ensure a total reflection at the surface of the fiber. From the ray-optic viewpoint, the resonance condition of the waveguide modes can be approximated as $n_2 L \approx n_2 \frac{2\pi}{\phi} x = p\lambda$. For the round trip length $L = 648 \mu\text{m}$ estimated from Fig. 5, the incident angle θ is calculated to be 66° , this value is in agreement with theory. Moreover, the waveguide modes are less confined at the liquid–capillary interface and the lasing emission can leak out of the inner cavity to the outer capillary as denoted by a red dotted line in the upper part of Fig. 6b. However, only a negligible portion of the lasing light could be reflected back into the inner cavity due

to the smaller incident angle at the external surface of the capillary, resulting in a weak modulation in the observed lasing peaks. From these two spectral changes, we

conclude that only the waveguide mode resonances are responsible for the weak-modulated lasing spectra shown in Fig. 5.

Fig. 6 Schematic representation of resonance modes supported in a capillary cavity without and with the central fiber

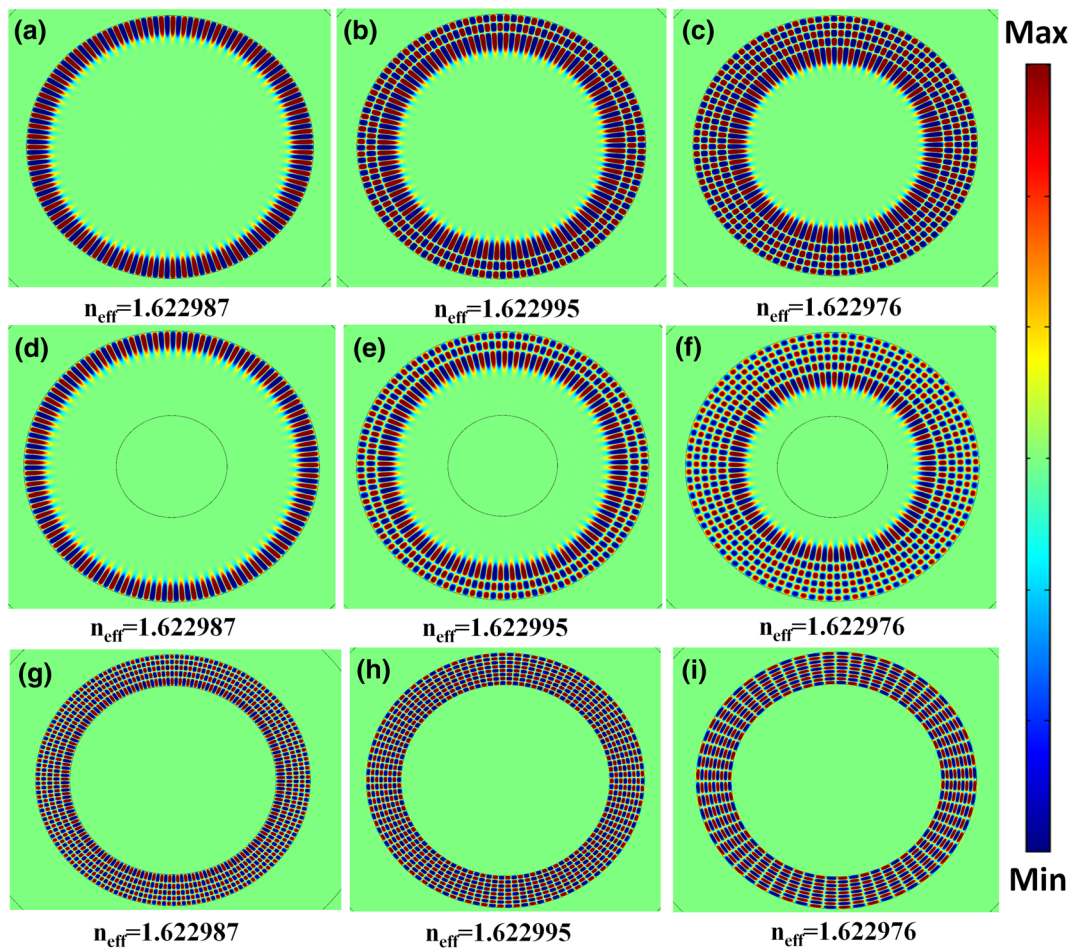
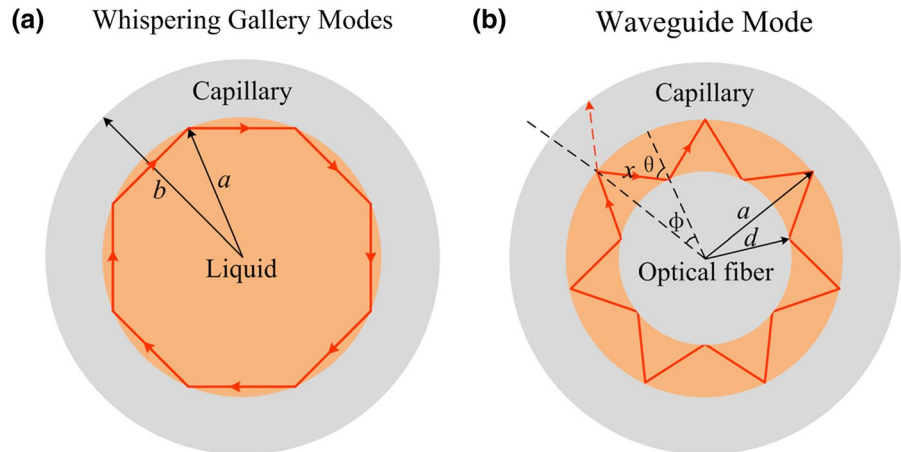


Fig. 7 Simulated electric field intensity distribution in the gain medium ($a = 80 \mu\text{m}$, $b = 120 \mu\text{m}$) with effective refractive index $n_{\text{eff}} = 1.622987$, 1.622995 , 1.622976 before (a–c) and after fiber insertion (d–i). Red (blue) regions in these panels depict positive

(negative) amplitudes of the electric field. Corresponding incident light $\lambda = 595 \text{ nm}$, and the inserted thin (d–f) and thick (g–i) fibers have radiuses d of 30 and $60 \mu\text{m}$, respectively

3.4 Simulated optical field distribution

In order to further demonstrate the lasing characteristics, 2D numerical simulations were carried out to evaluate the electric field distribution inside the capillary (inner radius $a \sim 80 \mu\text{m}$, outer radius $b \sim 120 \mu\text{m}$) using the time domain and frequency domain finite element methods. The electric field distribution inside a circular cross section of the gain medium is depicted for three of the resonances in Fig. 7a–c. Figure 7a shows the characteristic WGM pattern with $n_{\text{eff}} = 1.622987$ in which the optical field is well confined near the periphery of the gain medium due to the total internal reflection at the liquid–capillary interface. However, a clear standing wave field pattern induced by the feedback of the outer capillary is formed, as shown in Fig. 7b–c with $n_{\text{eff}} = 1.622995$ and 1.622976 , respectively. This is consistent with the experimental observation of the interference modulation lasing spectra.

For comparison, the same structure inserted by a low RI dielectric ($n_{\text{fiber}} = 1.45$) was also numerically modeled. When a comparatively thin fiber (radius $d = 30 \mu\text{m}$) was inserted in the capillary, the field distributions (Fig. 7d–f) are nearly identical to those obtained in the absence of fiber. As the fiber size increases ($d = 60 \mu\text{m}$), the field distribution (Fig. 7g–i) in the gain medium, in contrast, exhibits an extremely uniform standing wave pattern with the optical field located between the capillary wall and the fiber (rather than only along the circumference of the gain medium as would be expected for a fundamental WGM). The simulated results demonstrated in Fig. 7 indicate that without the central fiber or with a small size of the fiber inserted, the resonances are dominated by WGMs. When the size of the fiber increases to a certain amount of values, the resonances are dominated by waveguide modes as standing wave can be easily established between the capillary wall and the optical fiber. As mentioned above, a new inserted optical fiber system for modulating the microcavity resonant modes is presented.

4 Conclusion

In conclusion, we have demonstrated fluidic lasers based on capillary tubes. The lasers were simply and rapidly prepared by capillary action. An optical fiber was used to modulate the optically pumped lasing behaviors. The lasing characteristics and resonance mechanism of the two configurations were systematically discussed in both experiment and theoretical calculation. The conventional lasing without the central fiber was attributed to the whispering gallery resonances at the liquid–capillary interface, and the lasing spectra were modulated periodically due to the interference effect. With the central fiber inserted, the resonance

mechanism changed from WGMs to waveguide modes. The proposed waveguide model was experimentally verified by the analysis of (1) the mode spacing of the lasing peaks and (2) the weakened modulation in the observed lasing peaks, and further theoretically supported by the simulation using the finite element method. Owing to its easy fabrication, excellent laser performances and spectral modulation abilities, our system is a versatile candidate for extensive potential applications in optoelectronics devices.

Acknowledgments This work was supported by “973” Program (2011CB302004), NSFC (61275054), NSFC (11104119) and MOE (201110092130006).

References

1. H.M. Gibbs, G. Khitrova, S.W. Koch, Exciton-polariton light-semiconductor coupling effects. *Nat. Photonics* **5**, 275–282 (2011)
2. K.J. Vahala, Optical microcavities. *Nature* **424**, 839–846 (2003)
3. P. Rabeii, W.H. Steier, C. Zhang, L.R. Dalton, Polymer micro-ring filters and modulators. *J. Lightwave Technol.* **20**, 1968–1975 (2002)
4. J. Ward, O. Benson, WGM microresonators: sensing, lasing and fundamental optics with microspheres. *Laser Photonics Rev.* **5**, 553–570 (2011)
5. M.A. Santiago-Cordoba, S.V. Boriskina, F. Vollmer, M.C. Demirel, Nanoparticle-based protein detection by optical shift of a resonant microcavity. *Appl. Phys. Lett.* **99**, 073701 (2011)
6. J.P. Reithmaier, G. Sek, A. Löffler, C. Hofmann, S. Kuhn, S. Reitzenstein, L.V. Keldysh, V.D. Kulakovskii, T.L. Reinecke, A. Forchel, Strong coupling in a single quantum dot-semiconductor microcavity system. *Nature* **432**, 197–200 (2004)
7. G. Aubry, Q. Kou, J. Soto-Velasco, C. Wang, S. Meance, J.J. He, A.M. Haghiri-Gosnet, A multicolor microfluidic droplet dye laser with single mode emission. *Appl. Phys. Lett.* **98**, 111111 (2011)
8. R. Chen, Q.-L. Ye, T. He, V.D. Ta, Y. Ying, Y.Y. Tay, T. Wu, H. Sun, Exciton localization and optical properties improvement in nanocrystal-embedded ZnO core-shell nanowires. *Nano Lett.* **13**, 734–739 (2013)
9. R.-M. Ma, R.F. Oulton, V.J. Sorger, G. Bartal, X. Zhang, Room-temperature sub-diffraction-limited plasmon laser by total internal reflection. *Nat. Mater.* **10**, 110–113 (2011)
10. F. Todescato, I. Fortunati, S. Gardin, E. Garbin, E. Collini, R. Bozio, J.J. Jasieniak, G.D. Giustina, G. Brusatin, S. Toffanin, R. Signorini, Soft-lithographed up-converted distributed feedback visible lasers based on CdSe–CdZnS–ZnS quantum dots. *Adv. Funct. Mater.* **22**, 337–344 (2012)
11. J. Dai, C.X. Xu, K. Zheng, C.G. Lv, Y.P. Cui, Whispering gallery-mode lasing in ZnO microrods at room temperature. *Appl. Phys. Lett.* **95**, 241110 (2009)
12. V.D. Ta, R. Chen, L. Ma, Y.J. Ying, H.D. Sun, Whispering gallery mode microlasers and refractive index sensing based on single polymer fiber. *Laser Photonics Rev.* **7**, 133–139 (2013)
13. J. Schäfer, J.P. Mondia, R. Sharma, Z.H. Lu, A.S. Susha, A.L. Rogach, L.J. Wang, Quantum dot microdrop laser. *Nano Lett.* **8**, 1709–1712 (2008)
14. V.D. Ta, R. Chen, H.D. Sun, Tuning whispering gallery mode lasing from self-assembled polymer droplets. *Sci. Rep.* **3**, 1362 (2013)
15. S.I. Shopova, H. Zhou, X. Fan, P. Zhang, Optofluidic ring resonator based dye laser. *Appl. Phys. Lett.* **90**, 221101 (2007)
16. S.V. Frolov, M. Shkunov, Z.V. Vardeny, Ring microlasers from conducting polymers. *Phys. Rev. B.* **56**, 4363–4366 (1997)

17. T. Kobayashi, N. Byrne, Plastic evanescent microlaser. *Appl. Phys. Lett.* **99**, 153307 (2011)
18. H.-J. Moon, Y.-T. Chough, K. An, Cylindrical microcavity laser based on the evanescent-wave-coupled gain. *Phys. Rev. Lett.* **85**, 3161–3164 (2000)
19. I.M. White, H. Oveys, X. Fan, Liquid-core optical ring-resonator sensors. *Opt. Lett.* **31**, 1319–1321 (2006)
20. M. Saito, H. Shimatani, H. Naruhashi, Tunable whispering gallery mode emission from a microdroplet in elastomer. *Opt. Express* **16**, 11915–11919 (2008)
21. R. Chen, V.D. Ta, H. Sun, Bending-induced bidirectional tuning of whispering gallery mode lasing from flexible polymer fibers. *ACS Photonics* **1**, 11–16 (2014)
22. V.D. Ta, R. Chen, H. Sun, Coupled polymer microfiber lasers for single mode operation and enhanced refractive index sensing. *Adv. Optical Mater.* **2**, 220–225 (2014)
23. L. Shang, L. Liu, L. Xu, Single-frequency coupled asymmetric microcavity laser. *Opt. Lett.* **33**, 1150–1152 (2008)
24. X. Tu, X. Wu, M. Li, L. Liu, L. Xu, Ultraviolet single-frequency coupled optofluidic ring resonator dye laser. *Opt. Express* **20**, 19996–20001 (2012)
25. X. Wu, Y. Sun, J.D. Suter, X. Fan, Single mode coupled optofluidic ring resonator dye lasers. *Appl. Phys. Lett.* **94**, 241109 (2009)
26. S.K.Y. Tang, R. Derda, Q. Quan, M. Loncar, G.M. Whitesides, Continuously tunable microdroplet-laser in a microfluidic channel. *Opt. Express* **19**, 2204–2215 (2011)
27. H.-J. Moon, Y.-T. Chough, J.B. Kim, K. An, J. Yi, J. Lee, Cavity-Q-driven spectral shift in a cylindrical whispering-gallery-mode microcavity laser. *Appl. Phys. Lett.* **76**, 3679 (2000)
28. J. Haase, S. Shinohara, P. Mundra, G. Risse, V.G. Lyssenko, H. Fröb, M. Hentschel, A. Eychmuller, K. Leo, Hemispherical resonators with embedded nanocrystal quantum-rod emitters. *Appl. Phys. Lett.* **97**, 211101 (2010)
29. J.C. Knight, H.S.T. Driver, G.N. Robertson, Interference modulation of Q values in a cladded-fiber whispering-gallery-mode laser. *Opt. Lett.* **18**, 1296–1298 (1993)